bioRxiv preprint doi: https://doi.org/10.1101/2023.04.19.537509; this version posted April 21, 2023. The copyright holder for this preprint (which was not certified by peer review) is the author/funder, who has granted bioRxiv a license to display the preprint in perpetuity. It is made available under aCC-BY-NC-ND 4.0 International license.

Vimentin intermediate filaments structure and mechanically support microtubules in cells

Anna Blob,[†] David Ventzke,[†,‡] Giacomo Nies,[‡] Jan Niklas Dühmert,[¶] Bernhard Schmitzer,[¶] Axel Munk,[‡,§] Laura Schaedel,[‖] and Sarah Köster[*,†,§]

†*Institute for X-Ray Physics, University of Göttingen, Friedrich-Hund-Platz 1, 37077 Göttingen, Germany*

‡*Institute for Mathematical Stochastics, University of Göttingen, Goldschmidtstraße 7, 37077 Göttingen, Germany*

¶*Institute of Computer Science, University of Göttingen, Goldschmidtstraße 7, 37077 Göttingen, Germany*

§*Cluster of Excellence "Multiscale Bioimaging: from Molecular Machines to Networks of Excitable Cells" (MBExC), University of Göttingen, Germany*

‖*Department of Physics, Center for Biophysics, Saarland University, Campus A2 4, 66123 Saarbrücken, Germany*

E-mail: sarah.koester@uni-goettingen.de

Abstract

The eukaryotic cytoskeleton comprises three types of mechanically distinct biopolymers – actin filaments, microtubules and intermediate filaments (IFs)– along with passive crosslinkers and active molecular motors. Among these filament types, IFs are expressed in a cell-type specific manner and vimentin is found in cells of mesenchymal origin. The composite cytoskeletal network determines the mechanical and dynamic properties of the cell and is specifically governed by the interplay of the three different

bioRxiv preprint doi: https://doi.org/10.1101/2023.04.19.537509; this version posted April 21, 2023. The copyright holder for this preprint (which was not certified by peer review) is the author/funder, who has granted bioRxiv a license to display the preprint in perpetuity. It is made available under aCC-BY-NC-ND 4.0 International license.

filament systems. We study the influence of vimentin IFs on the mechanics and network structure of microtubules by analyzing fluorescence micrographs of fibroblasts on protein micropatterns. We develop and apply quantitative, automated data analysis to a large number of cells, thus mitigating the considerable natural variance in data from biological cells. We find that the presence of a vimentin IF network structures and aligns microtubules in the cell interior. On a local scale, we observe higher microtubule curvatures when vimentin IFs are present, irrespective of whether the cells are polarized or not. Our results suggest that the vimentin IF network laterally supports microtubules against compressive buckling forces and further helps to structure the microtubule network, thus possibly leading to a more efficient intracellular transport system along the microtubules.

Introduction

The cytoskeleton of eukaryotic cells consists of an intricate network of three types of biopolymers – actin filaments, microtubules and intermediate filaments (IFs) – along with cross linkers and molecular motors. Each of these biopolymers serves important functions in the cell and contributes specific mechanical and dynamic properties. Among these, microtubules are essential for cell division, intracellular transport and cell polarity[1], and vimentin IFs, some of the most abundant intermediate filaments, are strongly involved in cell migration, adhesion and maintaining the cell's mechanical integrity under external forces and deformations[2–4]. There is growing evidence that especially the interplay and interdependence of the different filament networks is of importance for the function of the cytoskeleton[5–7]. In this context, the interplay between stiff, inextensible microtubules and flexible, extremely extensible IFs is highly interesting[8]. Early on, colocalization and alignment of vimentin IFs and microtubules have been observed in different types of cells[9–11]. More specifically, vimentin IFs template the microtubule network in migrating cells[12] and help to maintain the cell polarity[13]. Consequently, knocking out IFs in cells can render the overall structure of the microtubule net-

bioRxiv preprint doi: https://doi.org/10.1101/2023.04.19.537509; this version posted April 21, 2023. The copyright holder for this preprint (which was not certified by peer review) is the author/funder, who has granted bioRxiv a license to display the preprint in perpetuity. It is made available under aCC-BY-NC-ND 4.0 International license.

work disorganized[14,15]. IFs, specifically vimentin and desmin IFs, can stabilize microtubules against depolymerization[12,16,17] and, vice versa, the stability of the intracellular vimentin IF network depends on microtubules: the network retracts to the perinuclear region upon microtubule network collapse[9,18]. Locally, the mechanical properties of microtubules are reflected by their bending caused by active, nonthermal forces[19–21]. Interestingly, they can resist large compressive forces in cells, by lateral support of the surrounding cytoskeletal matrix[22]. Indeed, for fibroblast cells, a larger buckling wavelength in vimentin-deficient cells has been observed[23] and there is a need for quantitative studies on statistically significant numbers of cells.

Here, we intend to gain deeper insight into the role of vimentin IFs in organizing and supporting microtubules in the intracellular space. Therefore, we investigate the influence of vimentin IFs on microtubules in mouse fibroblast cells with respect to the general network structure and the local curvatures. We include a large number of cells plated on predefined patterns in order to derive quantitative, statistically relevant data sets. We compare microtubule networks in NIH3T3 mouse fibroblast cells containing vimentin IFs and vimentin-knockout (vim-/-) mouse embryonic fibroblast cells, and find that the presence of vimentin IFs leads to alignment and radial orientation of the microtubules in the cell interior. Furthermore, by automatic segmentation of the microtubules and subsequent curvature analysis, we find that the curvature is correlated with the vimentin IF density. Our study highlights the importance of bias-free statistically relevant analysis that goes beyond effects that are directly visibly by eye and shows that vimentin IFs are essential for microtubule structure and organization on both the whole network scale and the local scale of individual microtubule shapes.

bioRxiv preprint doi: https://doi.org/10.1101/2023.04.19.537509; this version posted April 21, 2023. The copyright holder for this preprint (which was not certified by peer review) is the author/funder, who has granted bioRxiv a license to display the preprint in perpetuity. It is made available under aCC-BY-NC-ND 4.0 International license.

Materials and Methods

Experimental Methods

Micropatterning

Fibronectin micropatterns are prepared on glass coverslips (No 1.5H, Carl Roth, Karlsruhe, Germany) using the photopatterning system PRIMO (Alvéole, Paris, France) mounted on an inverted fluorescence microscope (IX83, Olympus, Tokyo, Japan) equipped with a 20x/NA 0.45 objective (LUCPLFLN 20x, Olympus). The glass coverslips are initially cleaned with isopropanol, blow-dried with N_2 and treated with air plasma (0.5 mbar at 50 W for 200s, ZEPTO, Diener Electronics GmbH, Ebhausen Germany). Polydimethylsiloxane (PDMS; Sylgard 184 Silicone Elastomer Kit, Dow, Midland, USA) stencils with a 3.5 mm diameter circular well are cleaned with isopropanol, blow-dried with N_2 and subsequently placed on the plasma-treated glass surface. The wells define the area that is patterned on each glass coverslip. Each well is filled with 0.1 mg/ml PLL-PEG (PLL(20)-g[3.5]-PEG(2), SuSoS AG, Dübendorf, Switzerland) in Dulbecco's Phophate Buffered Saline (PBS; Sigma-Aldrich, Merck KGaA, Darmstadt, Germany, #D8537) as passivation reagent and incubated for 1h at room temperature.

The wells are then rinsed three times with PBS followed by the addition of the UV-sensitive photo-initiator (4-benzoylbenzyl-trimethylammonium chloride, sold as PLPP (Product of Liaison for Protein Patterning) by Alvéole). Upon UV-illumination via the PRIMO module, this photo-intiator degrades the PLL-PEG passivation of the glass. The areas to be illuminated represent the patterns, in our case circles and crossbows, and are determined by a virtual mask, which is created with the open source software Inkscape and loaded into the PRIMO operating software Leonardo. After illuminating the sample wells with a UV dose of 1500 mJ/mm^2, they are washed three times with PBS, and fibronectin (from bovine plasma, Sigma-Aldrich, #F1141) with a concentration of 50 μg/ml in PBS is incubated for 1 to 2 h at room temperature or over night at 4°C. Unbound fibronectin is washed off by

bioRxiv preprint doi: https://doi.org/10.1101/2023.04.19.537509; this version posted April 21, 2023. The copyright holder for this preprint (which was not certified by peer review) is the author/funder, who has granted bioRxiv a license to display the preprint in perpetuity. It is made available under aCC-BY-NC-ND 4.0 International license.

rinsing the wells with PBS three times. The samples are stored in PBS for a maximum of two days at 4°C prior to seeding cells. To visually confirm the successful printing process, some patterns are prepared with 20% fluorescently labeled fibronectin (DyLight405). Labeling of the fibronectin is performed via an NHS-ester reaction with the amine groups in the protein (DyLight 405 Antibody Labeling Kit, Thermo Fisher Scientific, Waltham, MA, USA, #53020) following the manufacturer's protocol.

Cell culture

NIH3T3 mouse embryonic fibroblasts are purchased through DSMZ (ACC-59-NIH-3T3 fibroblasts, Leibniz Institute DSMZ - German Collection of Microorganisms and Cell Cultures GmbH, Braunschweig, Germany). The vimentin null mouse embryonic fibroblasts (vim-/-)[24] are kindly provided by Harald Herrmann (University Hospital Erlangen, Germany). Both cell lines are cultured in high glucose Dulbecco's Modified Eagle's Medium (Sigma-Aldrich, #D6429) supplemented with 10% of a serum substitute for fetal bovine serum (Fetal+, Serana, Pessin, Germany, #S-FBSP-EU-015), 1% GlutaMAX(Gibco, Thermo Fisher Scientific) and 1% penicillin-streptomycin (10,000 U/ml penicillin, 10 mg/ml streptomycin, PAN-Biotech, Aidenbach, Germany) at 37°C in a humidified incubator with 5% CO_2. NIH3T3 and vim-/- cells are subcultured every two to three days and every three to four days, respectively.

For seeding on fibronectin micropatterns, cells are treated with Trypsin/EDTA solution (0.05%/0.02% in PBS, PAN-Biotech¸, #P10-023100 for NIH3T3 and 0.25%/0.02% in PBS, PAN-Biotech, #P10-020100 for vim-/-) followed by centrifugation. The cell pellet is resuspended in medium and the cells are seeded with a density of $\sim 10\,000\,\mathrm{cells/cm^2}$ on the patterned glass slides with PDMS stencils. After 1 to 2 h, the PDMS stencils on the glass slides are removed and the glass slides with the attached cells are washed with full medium. In total, the cells grow on the patterns for 4h to 5h 15min before being fixed.

bioRxiv preprint doi: https://doi.org/10.1101/2023.04.19.537509; this version posted April 21, 2023. The copyright holder for this preprint (which was not certified by peer review) is the author/funder, who has granted bioRxiv a license to display the preprint in perpetuity. It is made available under aCC-BY-NC-ND 4.0 International license.

Fixation and immunofluorescence staining

Cells on micropatterns are chemically fixed and permeabilized by 4% formaldehyde (methanol-free, Thermo Scientific, #28906), 0.05% glutaraldehyde (Polysciences, Warrington, PA, USA, #01201) and 0.1% Triton X 100 in cytoskeleton buffer (9.3 mM MES, 128.34 mM KCl, 2.79 mM MgCl, 1.86 mM EGTA, adjusted to pH 6.1 with NaOH) with 9.3% sucrose. The samples are rinsed with PBS and subsequently incubated with $NaBH_4$ in PBS ($\sim$ 30 mM) for 10 min to reduce background fluorescence. After washing with PBS, the samples are incubated with a blocking solution consisting of 3% bovine serum albumin (BSA; Capricorn Scientific, Ebsdorfergrund, Germany, #BSA-1U) and 0.1% Tween 20 (Carl Roth, #9127.1) in PBS for 45 to 60 min at room temperature. Subsequently, the cells are incubated with primary antibodies against vimentin and tubulin diluted in blocking solution for 40 to 50 min at room temperature. After rinsing with PBS containing 0.1% Tween 20, the cells are incubated with secondary antibodies in blocking solution for 40 min at room temperature. After washing once more with PBS containing 0.1% Tween 20, the samples are briefly rinsed with ultra pure water and mounted on glass microscope slides with ProLong Glass Antifade Mountant (Invitrogen, Thermo Fisher Scientific, #P36982). In the case of samples with non-labeled fibronectin, the mountant contains Hoechst33342 (Mountant with NucBlue Stain, Invitrogen, #P36983). Thus, for each sample, we either fluorescently label the fibronectin pattern or we stain the nucleus.

As primary antibodies we use mouse monoclonal anti-α-tubulin (dilution 1:250, Invitrogen, #62204) and rabbit monoclonal anti-vimentin (D21H3) (dilution 1:200, Cell Signaling Technology, Danvers, MA, USA, #5741). As secondary antibodies we use goat anti-mouse Alexa Fluor 488 (dilution 1:500, Invitrogen, #A-11029) and goat anti-rabbit Alexa Fluor 647 (dilution 1:400, Abcam, Cambridge, UK, #ab150083).

bioRxiv preprint doi: https://doi.org/10.1101/2023.04.19.537509; this version posted April 21, 2023. The copyright holder for this preprint (which was not certified by peer review) is the author/funder, who has granted bioRxiv a license to display the preprint in perpetuity. It is made available under aCC-BY-NC-ND 4.0 International license.

Microscopy

Fluorescence images are recorded on an inverted laser scanning confocal microscope (Fluoview FV3000 on an IX83 microscope body, Olympus) equipped with a 60x/NA 1.4 oil objective (PLAPON-SC, Olympus) and the following laser lines: 405 nm, 488 nm and 640 nm. The 2D images of each cell are recorded at the lowest z-position within the cell where microtubules are in focus. Images of crossbow cells are taken such that the crossbows are oriented in parallel to the vertical axis of the image.

Image processing and data analysis

Only images of cells that are fully spread on patterns are considered. Additionally, we choose cells, where the microtubule density is low enough for further processing. All image processing is performed using self-written Python code.

Preprocessing of images

Initially, all cell images are aligned with respect to each other, in terms of position and orientation (see Fig. S1 in the Supplementary Material). Each aligned fluorescence image I of vimentin IFs or microtubules is normalized by subtracting the intensity minimum I_0 of the image and dividing by the 95% quantile intensity I_{95} of this background-corrected image:

$$I_{\text{norm}} = \frac{I - I_0}{I_{95}}.$$

Heatmaps showing the typical distribution of vimentin IFs in each cell category (NIH3T3 and vim-/-, circles and crossbows) are calculated by overlaying all normalized vimentin IF images of one category and calculating the mean intensity at each pixel.

Each cell of a category is segmented based on the background-subtracted microtubule image such that the resulting binary image I_{segm} consists of one connected cell interior and the outer surrounding. These segmented cells are overlaid and all pixels belonging to more than 10%

bioRxiv preprint doi: https://doi.org/10.1101/2023.04.19.537509; this version posted April 21, 2023. The copyright holder for this preprint (which was not certified by peer review) is the author/funder, who has granted bioRxiv a license to display the preprint in perpetuity. It is made available under aCC-BY-NC-ND 4.0 International license.

of all segmented cell areas constitute together a binary cell mask representing the typical cell area of that category (see Fig. S2 in the Supplementary Material). This binary cell mask is later used to define a clean cell edge for the representation of the alignment analysis and for the regional cell mask.

Microtubule skeletonization

To represent microtubules as a one-pixel-wide line, the aligned, normalized images of microtubules are binarized and skeletonized with Python code adapted from CytoSeg2.0.[25] In brief, the algorithm applies a "tubeness filter" that enhances filamentous structures, binarizes with an adaptive threshold, skeletonizes the binarized image and removes skeleton components that lie outside of the cell, have a low intensity in the fluorescence image or are smaller than a threshold size of 30 pixels. The necessary input parameters are manually chosen to achieve the best possible skeletonization of all cells with one global set of parameters upon visual inspection. See Fig. S3 in the Supplementary Material for a more detailed description of the worfklow for skeletonization and filament extraction.

Microtubule alignment and orientation analysis

The skeletonized microtubule images are analyzed with respect to the local degree of alignment of microtubules and their main orientation with Python code based on the AFT tool (Alignment by Fourier Transform) by Marcotti et al.[26]. In brief, we calculate a 2D fast Fourier transform (FFT) of overlapping subwindows of an image and perform a principal component analysis (PCA) on the norm of the FFT. With the resulting eigenvalues λ_1 and λ_2 of the covariance matrix of the image, the eccentricity $e = \sqrt{1 - \lambda_1/\lambda_2}$ is calculated as a measure for the degree of microtubule alignment with 0 indicating no alignment and 1 indicating maximum alignment. The orientation of the FFT norm and thus of the microtubules is determined as an angle between -90° and 90° with 0° corresponding to a horizontal orien-

bioRxiv preprint doi: https://doi.org/10.1101/2023.04.19.537509; this version posted April 21, 2023. The copyright holder for this preprint (which was not certified by peer review) is the author/funder, who has granted bioRxiv a license to display the preprint in perpetuity. It is made available under aCC-BY-NC-ND 4.0 International license.

tation in the image. Here, this analysis is applied with overlapping windows of size 71x71 pixels that slide along the image with steps of one pixel. For each window, the FFT norms of all cells are averaged before calculating the eccentricity and orientation.

Microtubule filament extraction and curvature analysis

The coordinates of the skeletonized microtubules are extracted by differentiating between intersections ("nodes"), endpoints and filament pixels based on the number of neighboring pixels. Connected filament pixels between two nodes or endpoints jointly constitute one "filament", which represents one segment of a real microtubule only, since the filament tracing does not continue across nodes. For simplicity, we still refer to these extracted segments as *filaments*.

For the curvature analysis only filaments longer than 20 pixels (=1.56 μm) are taken into account and their outer 3 pixels on each end are omitted to reduce the effect of skeletonization artifacts, which are more likely in dense node areas. The local curvature of the microtubules is determined by fitting an osculating circle to each filament pixel taking into account its neighboring pixels. In total $s = 13$ pixels contribute with weights that are given by a Gauss kernel truncated at two standard deviations. Therefore, for the fit to a pixel at position i_0 the 6 neighboring pixels to each side at position i are given a weight

$$w_i \propto \exp\left(-\frac{1}{2}\left(\frac{i - i_0}{(s-1)/4}\right)^2\right)$$

which is then divided by the sum of all weights to rescale the Gaussian kernel to 1. As a consequence, pixels contribute the less to the fit the further away they are from the pixel in question. At the end of a filament, depending on the pixel position, fewer than $s = 13$ pixels are taken into account for the fit. The fit is performed with the least-square method. The inverse of the circle radius corresponds to the curvature. To calculate a mean curvature, each curvature value is weighted by a simple approximation of the "length" of the corresponding

bioRxiv preprint doi: https://doi.org/10.1101/2023.04.19.537509; this version posted April 21, 2023. The copyright holder for this preprint (which was not certified by peer review) is the author/funder, who has granted bioRxiv a license to display the preprint in perpetuity. It is made available under aCC-BY-NC-ND 4.0 International license.

pixel. This accounts for the fact that a pixel represents a differently long part of a filament depending whether the pixel is in a vertical/horizontal or diagonal part of the microtubule. The "pixel length" is computed as $v = \sqrt{v_x^2 + v_y^2}$ with v_x as the central difference derivative of the filament pixel coordinates in x-direction and v_y as the central difference derivative in y-direction.

We estimate the mean microtubule curvature in dependence of the vimentin IF density by a sliding Gaussian window of standard deviation $h = 0.1$ density units that moves along the vimentin IF density axis. This means that for a given vimentin IF density we average the curvature value of all pixels, weighting them not only by the pixel length but also by the similarity of their vimentin IF density. Details on the averaging and the corresponding confidence band can be found in the Supplementary Material.

Histogram-based curvature analysis

For each cell and region we extract the full distribution of all curvatures observed within, see Fig. S4 in the Supplementary Material. Following Ref. 27 we represent each distribution by the inverse of its cumulative distribution function. Each of these cumulative distributions is an increasing function from $[0, 1]$ to (positive) curvature values, where $p \in [0, 1]$ is mapped to the p-quantile of the corresponding distribution. As shown in Ref. 27, this transformation is invertible and operations such as averaging and identifying dominant modes of variation on the transformed distributions better capture the structures in the data set, since it corresponds to a comparison of the distributions with the L^2-optimal transport metric. Numerically this transformation is implemented by first computing the cumulative distribution, approximating it by piecewise linear interpolation, and then sampling its inverse with $m = 10\,000$ points. This number is sufficiently high such that this procedure inflicts very little numerical error and yields indeed an approximately invertible transformation. We then apply a PCA in the transformed space for dimensionality reduction, i.e. we compute the empirical covariance matrix of the transformed samples and extract its dominant eigenvalues

bioRxiv preprint doi: https://doi.org/10.1101/2023.04.19.537509; this version posted April 21, 2023. The copyright holder for this preprint (which was not certified by peer review) is the author/funder, who has granted bioRxiv a license to display the preprint in perpetuity. It is made available under aCC-BY-NC-ND 4.0 International license.

and eigenvectors. Points in the transformed space can be transformed back to artificial distributions for visualization and interpretation of the directions that separate the two cell lines. We visualize the curvature distributions by binning them into discrete histograms, for which we divide the range from 0 to $3\mu\text{m}^{-1}$ into $n = 25$ bins of equal size and count for each bin the number of pixels within that range of curvatures. Re-transformed artificial distributions can sometimes contain slightly negative curvature values, which is a well-understood effect of the transform. For better visualization we truncate these values to zero in the histograms.

Results and discussion

To shed light on the influence of vimentin IFs on microtubules in cells, we investigate the network alignment as well as the local curvature of microtubules in mouse embryonic fibroblasts expressing vimentin (NIH3T3) and in vimentin-knockout mouse embryonic fibroblasts (vim-/-).[24,28] To render individual cells and their cytoskeletal networks comparable, we employ single-cell patterning and thus force the cells to take on defined shapes. We create circle- and crossbow-shaped fibronectin micropatterns, corresponding to unpolarized and polarized cells, respectively, as shown in Figs. 1A, B, in order to study a possible effect of cell shape and polarization. Thus, we analyze in total four categories of cells in this study: circle- and crossbow-shapes for NIH3T3 and vim-/- cells each. After chemical fixation and immunofluorescence staining of the cells on the patterns, the fluorescence intensity of microtubules and vimentin IFs is recorded using confocal microscopy for 95 to 105 cells per category; typical images are shown in Figs. 1C-F, with the microtubule networks represented in cyan and the vimentin IF networks shown in magenta. In NIH3T3 cells the vimentin IF network is located primarily in the cell center, i.e., close to the nucleus and is missing in the cell periphery. The microtubule network, by contrast, is spread out over the whole cells in both NIH3T3 and vim-/- cells. Individual microtubules are clearly distinguishable so that they are segmented and skeletonized as shown in Figs. 1G, H, K, L to facilitate the subsequent

bioRxiv preprint doi: https://doi.org/10.1101/2023.04.19.537509; this version posted April 21, 2023. The copyright holder for this preprint (which was not certified by peer review) is the author/funder, who has granted bioRxiv a license to display the preprint in perpetuity. It is made available under aCC-BY-NC-ND 4.0 International license.

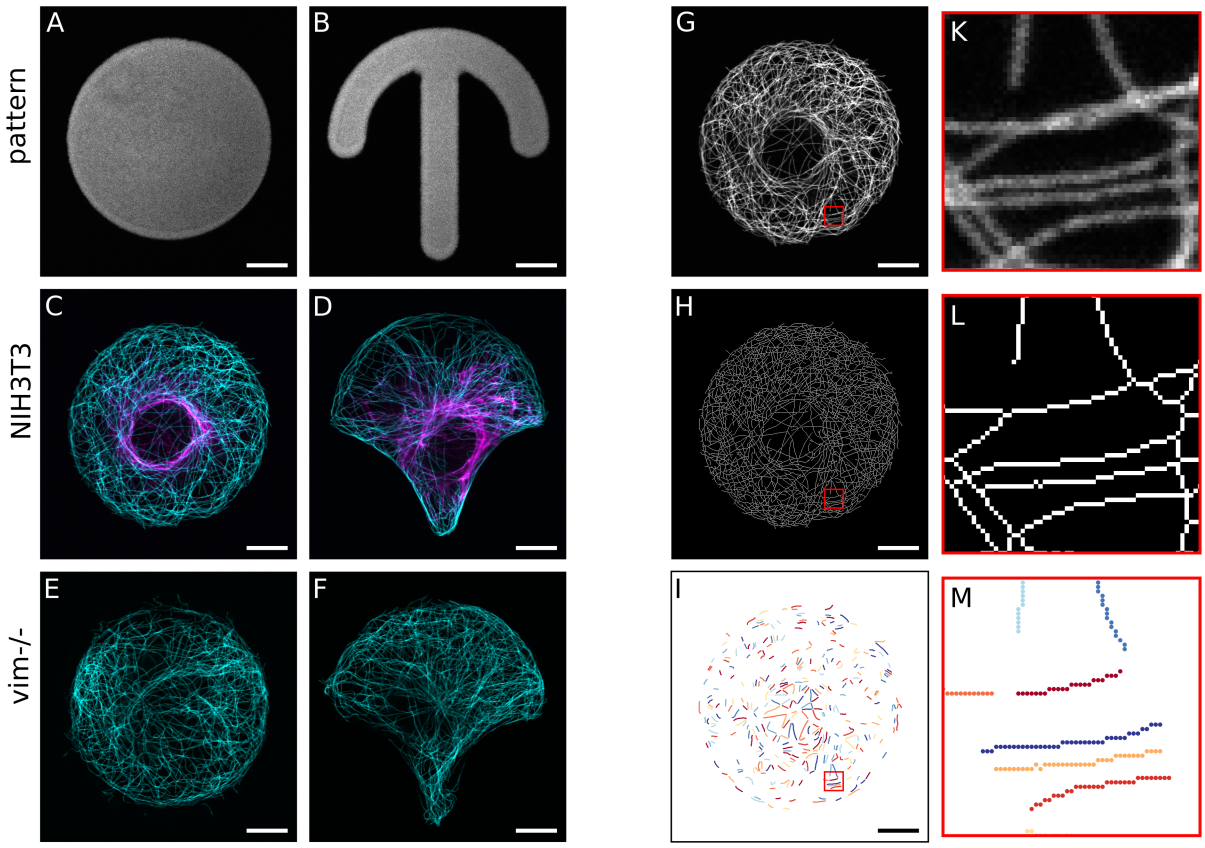

Figure 1: Microtubule and vimentin IF networks in cells on patterns. (A, B) Fibronectin patterns in the shape of a circle and crossbow. (C, D) Confocal microscopy images of fixed and antibody-stained single NIH3T3 cells on a circle and crossbow pattern. Microtubules are represented in cyan, vimentin IFs in magenta. (E, F) Confocal microscopy images of fixed and antibody-stained single vim-/- cells on a circle and crossbow pattern. (G) Fluorescence image of microtubules (same cell as in C). (H) Binarized and skeletonized microtubules from the image shown in (G). (I) Segments of extracted microtubule filaments from the skeleton shown in (H) that are used for curvature analysis (the different colors only serve to differentiate between different filaments). Scalebars: 10 μm. (K, L, M) Enlargements of the red marked regions in (G, H, I).

analysis of the network and individual filaments. In contrast, the vimentin IF network has a blurry appearance and single filaments are hardly visible. We attribute this difference to the smaller diameter of vimentin IFs (10 nm as compared to 25 nm for microtubules), their higher flexibility (persistence length of 2 μm as compared to several mm) and their higher propensity to form bundles and aggregates.

bioRxiv preprint doi: https://doi.org/10.1101/2023.04.19.537509; this version posted April 21, 2023. The copyright holder for this preprint (which was not certified by peer review) is the author/funder, who has granted bioRxiv a license to display the preprint in perpetuity. It is made available under aCC-BY-NC-ND 4.0 International license.

The vimentin IF network structures and aligns microtubules

Looking more closely at the fluorescence images of microtubules in cells, as shown in Figs. 1C-F, we observe a parallel alignment of the microtubules close to the rim of the cells. In order to investigate the microtubule network further, in particular in the cell interior, we analyze the alignment and orientation of skeletonized microtubules in a spatially resolved manner by FFT in sliding windows. Figs. 2A, B show the average alignment of microtubules in circular NIH3T3 and vim-/- cells and C, D show the alignment in crossbow-shaped cells. A high value (yellow) represents a strong alignment, with 1 for maximum alignment; a low value (blue) low alignment, with 0 for no alignment. In both cell types, the microtubules are, on average, strongly aligned at the cell edge. In the cell interior, however, there is a striking difference: in NIH3T3 cells, we observe a strong alignment, whereas in vim-/- cell, there is no such alignment.

The alignment does not reveal information about the direction of microtubule orientation within the cells. Therefore, we have a closer look at the actual orientation, see Figs. 2E-H. The color code represents the orientation angle with cyan for 0°, i.e., horizontal direction and red for the vertical direction. The orientation of the averaged cells along the rim looks alike, as for the alignment: the color code and thereby the orientation of the microtubules follows the tangential direction of the cell edge. In the cell interior, however, we observe a striking difference, which is more obvious for circle-shaped cells, in the orientation pattern between the cell lines. NIH3T3 cells show a "wheel" pattern, typical for radially oriented structures, which is missing entirely in vim-/- cells. The transition of radial to circumferential orientation in NIH3T3 circle-shaped cells explains the circular strip of low alignment that separates the inner region of the rim in Fig. 2A. For crossbow-shaped cells, the orientation patterns are overall similar between the cell lines with only the very center region being a bit less ordered in vim-/- cells. We speculate that in the crossbow-case the shape itself has a more dominant influence on the overall network structure than in the case of the rotationally symmetric circle-shape. Nevertheless, the orientation and alignment analyses together indicate that in

bioRxiv preprint doi: https://doi.org/10.1101/2023.04.19.537509; this version posted April 21, 2023. The copyright holder for this preprint (which was not certified by peer review) is the author/funder, who has granted bioRxiv a license to display the preprint in perpetuity. It is made available under aCC-BY-NC-ND 4.0 International license.

cells containing vimentin IFs the microtubule network is more structured and, specifically in circular cells, shows radial alignment.

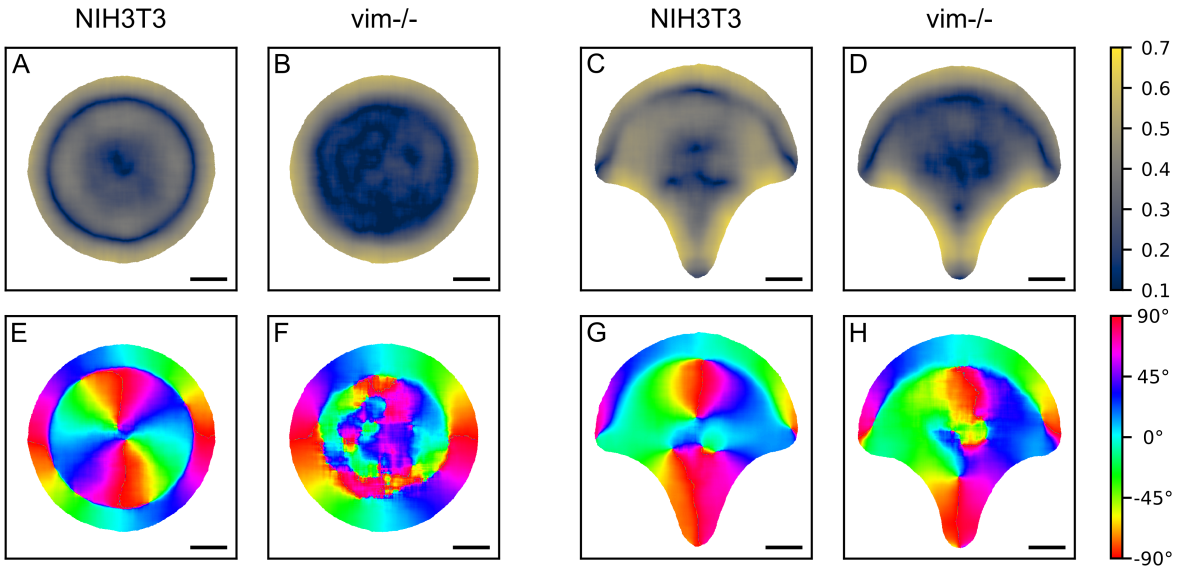

Figure 2: Influence of vimentin IFs on the structure of the microtubule network. (A, B, C, D) The averaged alignment of microtubules in circular cells with (A) and without (B) vimentin IFs and in crossbow-shaped cells with (C) and without (D) vimentin IFs, determined via Fourier analysis on skeletonized microtubule images. 0 corresponds to no alignment, 1 to maximum alignment. Whereas at the edge of the cells the microtubules are strongly aligned in both cell lines, the presence of vimentin IFs in NIH3T3 cells leads to alignment in the interior of the cell as well, which is missing in vim-/- cells. (E, F, G, H) The averaged main orientation of microtubules in circular cells (E, F) and in crossbow-shaped cells (G,H) with 0° describing a horizontal orientation. On the outer rim of both cell lines and cell shapes, the microtubules are oriented in parallel to the cell edge. In the interior of circular NIH3T3 cells the microtubules are clearly radially oriented, whereas in vim-/- cells there is no such structure.

The average microtuble curvature is independent of cell shape and presence of vimentin IFs

Beyond the orientation and alignment of microtubules, their local curvatures provide information about a possible role of the surrounding cytoskeletal matrix in the mechanical support of microtubules[20]. We therefore extract the coordinates of skeletonized microtubules and analyze the local curvatures. We only consider the center parts of microtubule segments longer

bioRxiv preprint doi: https://doi.org/10.1101/2023.04.19.537509; this version posted April 21, 2023. The copyright holder for this preprint (which was not certified by peer review) is the author/funder, who has granted bioRxiv a license to display the preprint in perpetuity. It is made available under aCC-BY-NC-ND 4.0 International license.

than 1.56 μm between crossing points (referred to as *filaments*) as shown in Figs. 1I, M to minimize the influence of skeletonization artifacts in dense network areas. The curvature value for each pixel of a filament is determined by fitting a circle to its surrounding pixels as illustrated in the inset of Fig. 3.

Fig. 3 shows the distributions of the means of all curvature values within each individual cell. For crossbow shapes, NIH3T3 cells show a median average curvature of 0.616 μm^{-1} versus 0.622 μm^{-1} for vim-/- cells which corresponds to a difference of less than 1 %. For circle shapes, NIH3T3 cells yield a median average curvature of 0.636 μm^{-1} versus 0.619 μm^{-1} for vim-/- cells, corresponding to a difference of 2.7 % with NIH3T3 cells containing the larger curvature. In order to investigate this small difference further, we continue with a more detailed regional analysis as the average over an entire cell does not account for the complex, heterogeneous interior of cells, where different regions show highly different structure, dynamics and thus present differing environments to the microtubules investigated here.

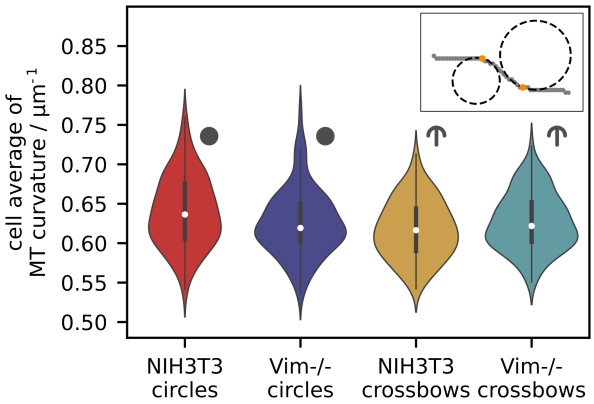

Figure 3: Distribution of cellular averages of the microtubule curvature. Inset: example filament and curvature determination by circle fitting at the two pixels marked in orange. For each individual cell, the mean of all curvature values is calculated. The distribution of these cellular means is represented for each cell category in a violin plot with the median marked by a white circle. The thick black line represents the interquartile range. There are only small differences of microtubule curvature between cell lines and shapes.

bioRxiv preprint doi: https://doi.org/10.1101/2023.04.19.537509; this version posted April 21, 2023. The copyright holder for this preprint (which was not certified by peer review) is the author/funder, who has granted bioRxiv a license to display the preprint in perpetuity. It is made available under aCC-BY-NC-ND 4.0 International license.

Microtubule curvature and vimentin density vary locally

In order to account for the intracellular heterogeneity, we further analyze the microtubule curvature in different cell regions taking into account the corresponding vimentin IF density. The heatmaps in Figs. 4A, B represent the average vimentin IF distribution in circle- and crossbow-shaped NIH3T3 cells. In circle-shaped cells, vimentin IFs form a dense network around the nucleus area in the center that decreases continuously going outwards so that at the very periphery of the cell almost no vimentin IFs are present, in agreement with previously published data on mouse fibroblasts.[13] In crossbow-shaped cells, vimentin IFs show a similar density decrease towards the periphery of the arch and the pointed edge of the crossbow, whereas the dense encirclement of the nucleus is not as pronounced as for the circle-shaped cells. The maximum amount of vimentin IFs is located next to the nucleus but only on the side facing the arched cell edge. These vimentin IF distributions serve as a basis for creating masks that are applied to all cells, both NIH3T3 and vim-/-, of the same shape. The masks, one for circle-shaped cells and one for crossbow-shaped cells, are constructed such that each of the 9 regions represents pixels belonging to a certain interval of the total intensity of the vimentin IF heatmap. As shown in Figs. 4C, D, region 1 (yellow) corresponds to the cell location with the highest average vimentin IF content in NIH3T3 cells, and region 9 (dark purple) to the outer-most periphery of the cell, where there are the least vimentin IFs found on average.

For each cell shape, the corresponding mask is applied to each individual cell to calculate the mean of the vimentin IF intensity or of the microtubule curvature. The medians of the distributions of these cellular means are plotted against the cell regions in Figs. 4E-H. The median absolute deviations (MADs) are shown as error bars and provide a measure for the spread of the data. Consistent with the mask creation procedure that is based on the vimentin IF distribution, the averaged vimentin IF intensity decreases approximately linearly from the near-center region 1 to region 9 for both circle and crossbow-shaped NIH3T3 cells, as shown in Figs. 4E, F. Interestingly, averaging all values of microtubule curvature and

bioRxiv preprint doi: https://doi.org/10.1101/2023.04.19.537509; this version posted April 21, 2023. The copyright holder for this preprint (which was not certified by peer review) is the author/funder, who has granted bioRxiv a license to display the preprint in perpetuity. It is made available under aCC-BY-NC-ND 4.0 International license.

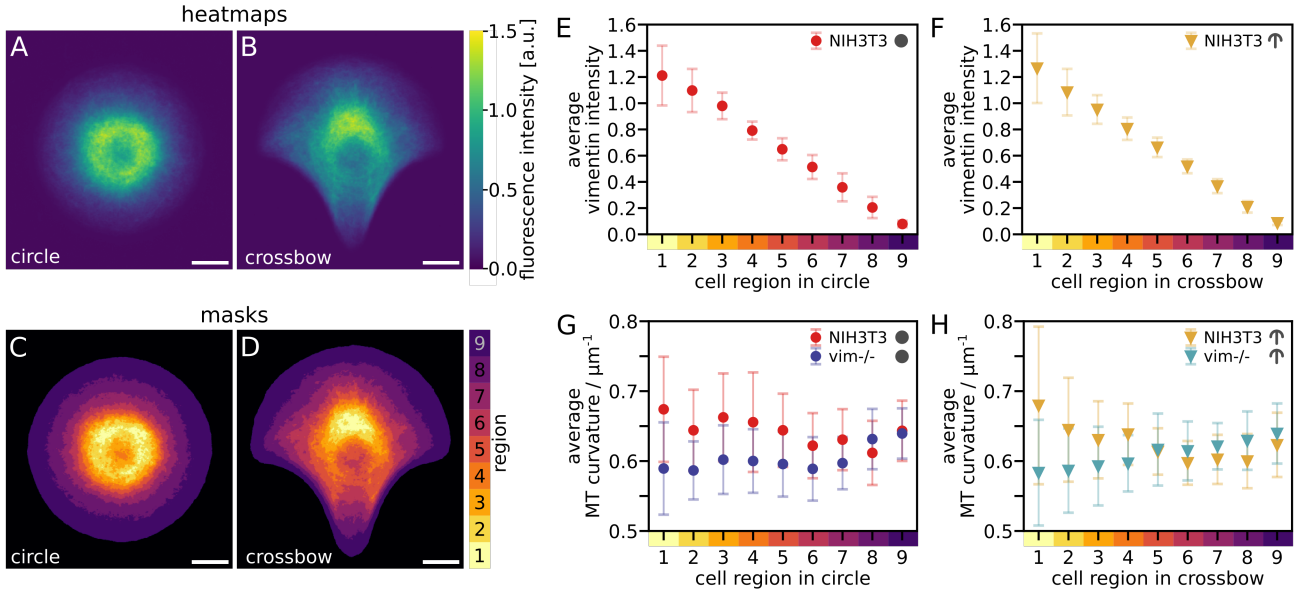

Figure 4: Regional analysis of vimentin IF density and microtubule curvature. (A, B) Vimentin IF heatmaps generated by averaging the vimentin IF fluorescence intensity of all NIH3T3 cells on circles and crossbows. (C, D) Masks for circles and crossbows dividing the cell into 9 regions based on the average vimentin IF distribution in NIH3T3 cells. Scalebars: 10 μm. (E, F) Average vimentin IF fluorescence intensity in the different regions for NIH3T3 cells on circle and crossbow patterns. The approximately linear decrease stems from the regional division being based on the vimentin IF distribution. (G, H) Average microtubule (MT) curvature in the different regions of NIH3T3 and vim-/- cells in circle and crossbow shape. In the center regions, where NIH3T3 cells contain more vimentin IFs than in outer regions, the microtubule curvature is higher in NIH3T3 cells than in vim-/- cells. Each data point in (E) to (H) represents the median of the cellular mean values with the median absolute deviation (MAD) as errorbar.

comparing between NIH3T3 and vim-/- cells (see Figs. 4G, H) reveals regional differences. For circle-shaped cells (Fig. 4G), in the outer-most region 9, where NIH3T3 cells possess almost no vimentin IFs, the microtubule curvature is nearly identical for both cell lines. Moving towards the inner regions with increasingly more vimentin IFs in NIH3T3 cells, the difference in microtubule curvature between the cells with and without vimentin IFs increases. Whereas the curvature for vim-/- cells (dark blue) slightly decreases and then more or less stagnates going from region 9 to region 1, the curvature of NIH3T3 cells (red) slightly increases overall. A similar trend is observed for crossbow-shaped cells, presented in Fig. 4H. For vim-/- cells (light blue), the microtubule curvature decreases from region

bioRxiv preprint doi: https://doi.org/10.1101/2023.04.19.537509; this version posted April 21, 2023. The copyright holder for this preprint (which was not certified by peer review) is the author/funder, who has granted bioRxiv a license to display the preprint in perpetuity. It is made available under aCC-BY-NC-ND 4.0 International license.

9 to region 1. For NIH3T3 cells (orange), in the outer regions 9 to 6 the microtubule curvature is similar to that of vim-/- cells or even slightly smaller. However, from region 5 going towards regions 1 the curvature becomes larger for NIH3T3 cells. Thus, the maximum difference in microtubule curvature between the cell lines is found in region 1 which contains most vimentin IFs in NIH3T3 cells. From this regional analysis and comparison of the microtubules curvature, we see that indeed there is a difference between the cells with and without vimentin IFs which is not visible when averaging over the entire cell. Generally, the microtubule curvature of NIH3T3 cells in regions with a lot of vimentin IFs is higher than in the corresponding regions in vim-/- cells whereas there is little difference in regions where NIH3T3 cells have only few vimentin IFs anyway. This indicates an influence of the presence of vimentin IFs on the curvature of microtubules.

Histogram-based curvature analysis confirms influence of vimentin IF network

In order to take into account the distributions of curvature beyond average values as in the previous section, we extract the corresponding curvature histogram for each cell and region. 80 typical histograms each of circle-shaped NIH3T3 (red) and vim-/- (blue) cells are shown in Figs. 5A, B for region 1 and 9. We then compute the inverse cumulative distribution functions of all histograms and apply a PCA on the transformed space. The first two principal components account for approximately $73.5\% + 15.7\% = 89.2\%$ of the variance and thus provide a useful basis for dimensionality reduction. Figs. 5C, D show the projection of the (transformed) histograms from regions 1 and 9 of all circle-shaped cells onto the two leading principal components and stars and ellipsoids that represent the mean and covariance matrices of the projected point clouds for the two cell types. In region 1 the means of the two different cell types are separated by approximately one standard deviation, whereas in region 9 the separation is less pronounced.

Since the inverse cumulative distribution transformation is invertible, arbitrary points in the

bioRxiv preprint doi: https://doi.org/10.1101/2023.04.19.537509; this version posted April 21, 2023. The copyright holder for this preprint (which was not certified by peer review) is the author/funder, who has granted bioRxiv a license to display the preprint in perpetuity. It is made available under aCC-BY-NC-ND 4.0 International license.

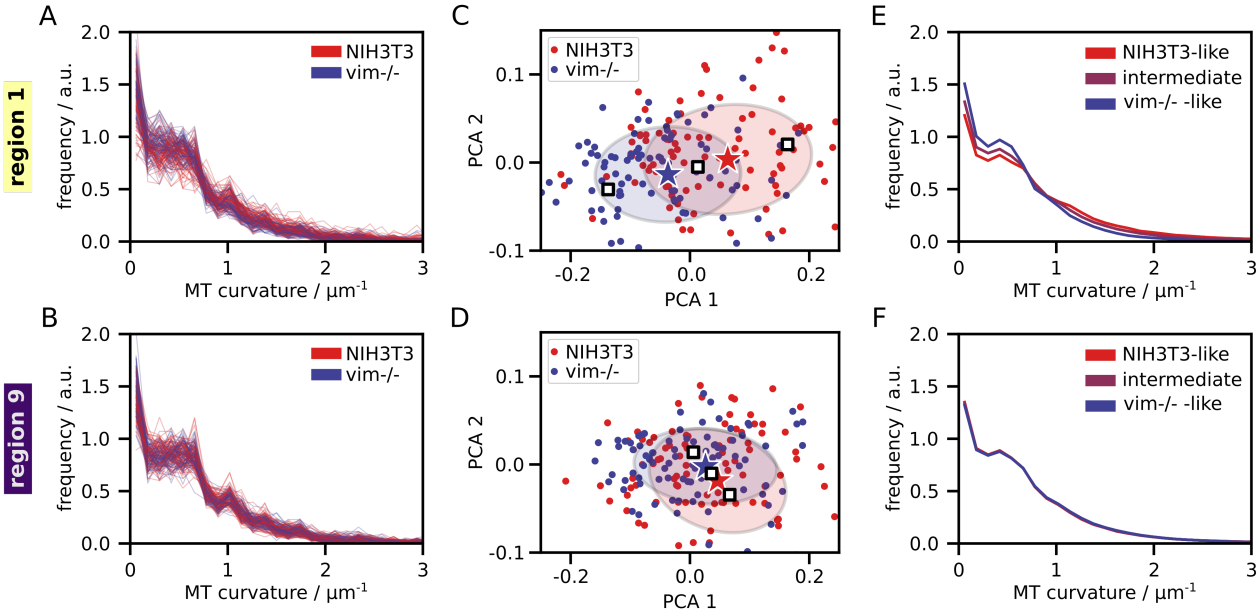

Figure 5: Region dependent analysis of curvature histograms on circle cells. (A,B) 80 example histograms each for curvatures from circle-shaped NIH3T3 (red) and vim-/- (blue) cells for region 1 and 9. The vertical axis gives the normalized observed frequency of a given curvature. (C,D) PCA embedding onto two leading modes of NIH3T3 and vim-/- histograms from regions 1 and 9. Each point is calculated from the histogram of one cell. Stars and ellipsoids indicate the mean and covariance of each point cloud. The center square marker lies in the middle between the two stars and the distance of the outer markers to the nearest star is equal to the distance between the stars. (E,F) Reconstructed histograms corresponding to square markers in (C,D) illustrating the transition between prototypical NIH3T3 and vim-/- histograms. For region 1 the vim-/- histogram exhibits higher densities at low curvatures, for region 9 the histograms are essentially identical.

plane plotted in Figs. 5C, D can be transformed back to a histogram. Fig. 5E shows three such histograms for region 1, corresponding to the squares marked in Fig. 5C. The marker in the center lies in the middle between the two stars. The two outer markers correspond to “NIH3T3-like" or “vim-/- -like” cells. The distance of the outer markers to the nearest star is equal to the distance between the stars. Thus, moving along the three markers corresponds to the transition between representative samples of NIH3T3 and vim-/- cells. In Fig. 5E, for region 1, we observe that the histogram corresponding to the vim-/- cells has a higher density of low curvatures and a lower density of high curvatures, as compared to the NIH3T3 cells. In Fig. 5F, for region 9, there is no discernible difference between the histograms of the two cell types. These trends are consistent with the spectrum of variations shown in

bioRxiv preprint doi: https://doi.org/10.1101/2023.04.19.537509; this version posted April 21, 2023. The copyright holder for this preprint (which was not certified by peer review) is the author/funder, who has granted bioRxiv a license to display the preprint in perpetuity. It is made available under aCC-BY-NC-ND 4.0 International license.

Figs. 5A, B. These findings are in agreement with the analysis of the previous section where we compare curvature averages. For the histogram-based PCA we take into consideration the entire curvature distribution instead of average values as above. Thus, these findings strongly support the hypothesis that the presence of a vimentin IF network leads to a higher microtubule curvature.

Microtubule curvature depends on local vimentin IF density

As the data of the regional curvature analysis of the two previous sections indicate a correlation between the density of vimentin IFs and microtubule curvature, we investigate this correlation in more detail by performing a local analysis for each image pixel in NIH3T3 cells. We apply a small Gaussian kernel with a standard deviation of $0.23\,\mu$m to the microscopy images of vimentin IFs so that the intensity at each pixel can be considered as a measure of the density of the vimentin IF network. Each skeletonized microtubule pixel analyzed with regard to its curvature (see above) can now be related to its corresponding vimentin IF density. For each cell category, this yields on the order of 600 000 pairs of data points to which we apply a moving average to investigate correlations between density and curvature despite a large natural variance of the data. The averaging procedure provides the weighted mean of curvature values belonging to pixels with weights defined by a Gaussian window of standard deviation $h = 0.1$ density units on the vimentin IF density axis. The averaging Gaussian kernel moves along the vimentin IF density axis in steps of 0.05 density units.

This moving average reveals a clear correlation between the microtubule curvature and the vimentin IF density as shown in Fig. 6. With increasing vimentin IF density we observe an increasing microtubule curvature for both circle and crossbow-shaped NIH3T3 cells. The curves are represented with a 95% pointwise confidence interval each, which becomes larger towards higher vimentin IF density values as the number of data points decreases drastically from low to high densities. As the trend of rising microtubule curvature with vimentin IF density is the same for both crossbow- and circle-shaped cells, we conclude that it is cell

bioRxiv preprint doi: https://doi.org/10.1101/2023.04.19.537509; this version posted April 21, 2023. The copyright holder for this preprint (which was not certified by peer review) is the author/funder, who has granted bioRxiv a license to display the preprint in perpetuity. It is made available under aCC-BY-NC-ND 4.0 International license.

geometry-independent. The curvature values we measure are on the order of 0.7 μm^{-1}. Thus, the average radius of curvature is on the order of 1.4 μm, highlighting the strong nonthermal, active forces that act on microtubules in cells and make them bend so strongly despite a persistence length of several mm.

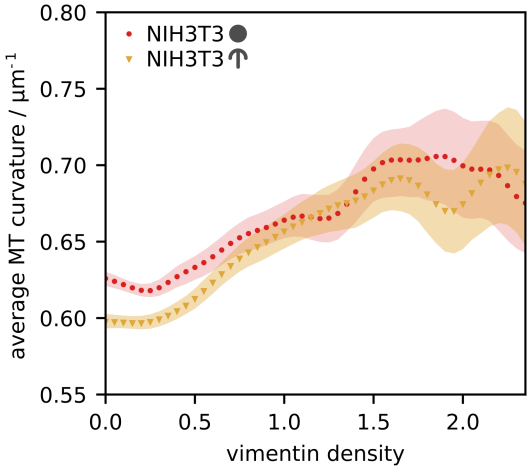

Figure 6: Microtubule curvature depends on the density of vimentin IFs. Average microtubule curvature in dependence of vimentin IF density in NIH3T3 cells (moving average with weights given by a Gaussian kernel with standard deviation of 0.1 density units). Each curve is represented with a 95% pointwise confidence band. The number of data points decreases with increasing vimentin IF density and is thus responsible for high noise towards higher densities. The plot includes data ranges up to the point where the width of the confidence band of both categories is higher than 10% of the average curvature. The microtubule curvature increases with increasing vimentin IF density.

Discussion and conclusion

We study the influence of the vimentin IF network on the microtubule network in mouse fibroblasts. These cells are chosen for their wide-spread use in a variety of studies and their biological importance as typical cells of mesenchymal origin. As fibroblasts are migrating cells and thus polarize in order to perform directional movement, we perform our experiments on both non-polarized, circular patterns and on polarized, crossbow patterns. However, in our analysis, we find only small shape-effects with regard to alignment and no effects with regard to curvature analysis. In order to investigate the effect of the presence or absence

bioRxiv preprint doi: https://doi.org/10.1101/2023.04.19.537509; this version posted April 21, 2023. The copyright holder for this preprint (which was not certified by peer review) is the author/funder, who has granted bioRxiv a license to display the preprint in perpetuity. It is made available under aCC-BY-NC-ND 4.0 International license.

of a vimentin IF network, we perform our study on NIH3T3 cells with vimentin IFs and on vim-/- cells without vimentin IFs and observe strong differences between the two cell lines. Beyond earlier studies of microtubule distribution using heatmaps[13], our approach to analyze the orientation and alignment of microtubules reveals additional information regarding local network organization. In circular cells containing vimentin IFs, the microtubule network is radially aligned pointing from the nucleus outwards to the cell rim. Intuitively, radially organized microtubules provide a more ordered "track" system for intracellular transport and this increased order may be beneficial for the cell for efficient distribution of intracellular components, vesicles and small organelles. Thus, our results indicate that vimentin IFs indirectly support intracellular transport via microtubules. Our results are in agreement with previous studies in mouse cardiomyocytes, where knocking out desmin, an IF protein similar to vimentin, but found in muscle cells, renders the microtubule network less organized[14]. Our findings are in line with the role of vimentin IFs for cell polarity[12,13] and the enhancement of centrosome-mediated microtubule growth by vimentin IFs[29]. Together, these results contribute to a consistent picture of vimentin IFs as an essential structuring element for the cell interior and its microtubule network.

In addition to the overall increased microtubule alignment and very distinct radial organization, we observe an influence of the vimentin IF network, which surrounds the microtubules as a viscoelastic matrix, on the microtubule bending. The order of magnitude of our measured curvature values is nicely in line with previous literature on microtubule shapes in cells[21,30,31]. The effect of the vimentin IF network becomes visible when analyzing the microtubule bending in a spatially resolved manner. The bending of microtubules in cells with vimentin is stronger than in cells without vimentin but only in those regions with a high vimentin IF density. The local correlation between vimentin IF density and microtubule curvature in cells expressing vimentin complements the regional comparison of our two cell lines confirming that indeed vimentin creates a curvature difference between the cell lines. Thus, our systematic, quantitative study agrees with the observation of larger wavelength-buckling

bioRxiv preprint doi: https://doi.org/10.1101/2023.04.19.537509; this version posted April 21, 2023. The copyright holder for this preprint (which was not certified by peer review) is the author/funder, who has granted bioRxiv a license to display the preprint in perpetuity. It is made available under aCC-BY-NC-ND 4.0 International license.

in vim-/- cells by Alisafaei et al.[23] and the cryo-electron tomography study by Chacraborty et al.[32] who find that microtubules in HeLa and P19 cells are more curved when entangled with IFs or actin. However, the relationship between microtubules and vimentin IFs might be celltype-dependent, as in *X. laevis* melanophores a decrease of the apparent persistence length, which is equivalent to higher curvatures, was observed without vimentin IFs[33]. Our observation of increased microtubule curvature with local vimentin IF density can be understood as follows: The presence of a (denser) vimentin IF networks leads to an increased elastic modulus of the cytoplasm[34] and serves as a matrix surrounding the microtubules that experience high compressive forces and thus buckle. Due to minimization of the total mechanical energy (microtubule bending and matrix deformation), buckling in such an elastic matrix occurs with a smaller buckling wavelength, and thus higher curvature, than in a purely viscous fluid[22]. Thus, the (locally) increased elastic modulus of cells containing vimentin IFs leads to smaller wavelengths, which we observe as higher curvatures.

Clearly, apart from the vimentin IF network, there are additional cell region-dependent factors that may influence microtubule organization and mechanics, such as the actin network, which certainly contributes to the viscoelasticity of the surrounding matrix, as well as the nucleus and other organelles that take up space in the cytoplasm. Yet, varying the cell shape also changes the distribution of these region-dependent factors and the cell shape-independence of our findings regarding microtubule curvature indicates that the correlation with the vimentin IF density is independent of these other factors.

In conclusion, our study shows that the vimentin IF network in fibroblasts plays an important role for the microtubule network in several respects: the dense vimentin IF network with a small mesh size provides a "quasi-continuous" matrix in which the microtubules dynamically grow. As a consequence, they (i) are pointing radially outwards from the cell center, i.e., close to the nucleus, to the cell periphery and thus provide a very structured and efficient track system for intracellular transport. A similar "ordering element" is provided by the cell edge, independent of the presence of vimentin IFs. (ii) By increased elasticity, the

bioRxiv preprint doi: https://doi.org/10.1101/2023.04.19.537509; this version posted April 21, 2023. The copyright holder for this preprint (which was not certified by peer review) is the author/funder, who has granted bioRxiv a license to display the preprint in perpetuity. It is made available under aCC-BY-NC-ND 4.0 International license.

vimentin matrix leads to decreased buckling wavelengths, equivalent to higher curvatures, of the microtubules. Our systematic analysis on a large number of cells reveals these effects in a very clear manner, although they are not visible when looking at a small number of individual cells. This emphasizes the importance of studies on large cell ensembles, which account for a pronounced cell-to-cell variability and the use of tools that impose boundary conditions such as cell shape and size.

Acknowledgement

We thank Ulrike Rölleke, Charlotta Lorenz, Anna V. Schepers, Alexander Egner, Jan Christoph Thiele, Harald Herrmann, Alexandre Schaeffer, Manuel Théry, Susanne Hengst and Gilles Mordant for fruitful discussions and technical support. The vim-/- cells were kindly provided by Harald Herrmann. This work was funded by the Deutsche Forschungsgemeinschaft (DFG, German Research Foundation) – Project-ID 432680300 – SFB 1456 project A04 (to S.K. and A.M.) and A03 (to B.S.) and under Germany's Excellence Strategy (EXC 2067/1-390729940 to S.K. and A.M.). The work was further financially supported by the European Research Council (ERC, Grant No. CoG 724932, to S.K.).

Author contributions

S.K., L.S., A.M. and B.S. designed research and supervised this work; A.B. performed experiments; A.B., D.V., G.N. and J.N.D. analyzed data; A.B. and S.K. wrote the original draft of the paper; all authors edited and reviewed the paper.

Competing interests

The authors declare no competing interests.

bioRxiv preprint doi: https://doi.org/10.1101/2023.04.19.537509; this version posted April 21, 2023. The copyright holder for this preprint (which was not certified by peer review) is the author/funder, who has granted bioRxiv a license to display the preprint in perpetuity. It is made available under aCC-BY-NC-ND 4.0 International license.

Supporting Citations

References 25,35,36, appear in the Supplementary Material.

References

(1) Garcin, C.; Straube, A. Microtubules in cell migration. *Essays Biochem.* **2019**, *63*, 509–520.

(2) Mendez, M. G.; Kojima, S.; Goldman, R. D. Vimentin induces changes in cell shape, motility, and adhesion during the epithelial to mesenchymal transition. *FASEB J.* **2010**, *24*, 1838–1851.

(3) Etienne-Manneville, S. Cytoplasmic Intermediate Filaments in Cell Biology. *Annu. Rev. Cell Dev. Biol.* **2018**, *34*, 1–28.

(4) Hu, J.; Li, Y.; Hao, Y.; Zheng, T.; Gupta, S. K.; Parada, G. A.; Wu, H.; Lin, S.; Wang, S.; Zhao, X.; Goldman, R. D.; Cai, S.; Guo, M. High stretchability, strength, and toughness of living cells enabled by hyperelastic vimentin intermediate filaments. *Proc. Natl. Acad. Sci. USA* **2019**, *116*, 17175–17180.

(5) Huber, F.; Boire, A.; López, M. P.; Koenderink, G. H. Cytoskeletal crosstalk: when three different personalities team up. *Curr. Opin. Cell Biol.* **2015**, *32*, 39–47.

(6) Chang, L.; Goldman, R. D. Intermediate filaments mediate cytoskeletal crosstalk. *Nat. Rev. Mol. Cell Biol.* **2004**, *5*, 601–613.

(7) Wu, H.; Shen, Y.; Sivagurunathan, S.; Weber, M. S.; Adam, S. A.; Shin, J. H.; Fredberg, J. J.; Medalia, O.; Goldman, R.; Weitz, D. A. Vimentin intermediate filaments and filamentous actin form unexpected interpenetrating networks that redefine the cell cortex. *Proc. Natl. Acad. Sci. USA* **2022**, *119*, e2115217119.

bioRxiv preprint doi: https://doi.org/10.1101/2023.04.19.537509; this version posted April 21, 2023. The copyright holder for this preprint (which was not certified by peer review) is the author/funder, who has granted bioRxiv a license to display the preprint in perpetuity. It is made available under aCC-BY-NC-ND 4.0 International license.

(8) Wen, Q.; Janmey, P. A. Polymer physics of the cytoskeleton. *Curr. Opin. Solid State Mater. Sci.* **2011**, *15*, 177–182.

(9) Goldman, R. D. The role of three cytoplasmic fibers in BHK-21 cell motility. *J. Cell Biol.* **1971**, *51*, 752–762.

(10) Ball, E. H.; Singer, S. J. Association of microtubules and intermediate filaments in normal fibroblasts and its disruption upon transformation by a temperature-sensitive mutant of Rous sarcoma virus. *Proc. Natl. Acad. Sci. USA* **1981**, *78*, 6986–6990.

(11) Nieuwenhuizen, R. P. J.; Nahidiazar, L.; Manders, E. M. M.; Jalink, K.; Stallinga, S.; Rieger, B. Co-Orientation: Quantifying Simultaneous Co-Localization and Orientational Alignment of Filaments in Light Microscopy. *PLoS One* **2015**, *10*, e0131756.

(12) Gan, Z.; Ding, L.; Burckhardt, C. J.; Lowery, J.; Zaritsky, A.; Sitterley, K.; Mota, A.; Costigliola, N.; Starker, C. G.; Voytas, D. F.; Tytell, J.; Goldman, R. D.; Danuser, G. Vimentin Intermediate Filaments Template Microtubule Networks to Enhance Persistence in Cell Polarity and Directed Migration. *Cell Syst.* **2016**, *3*, 252–263.

(13) Shabbir, S. H.; Cleland, M. M.; Goldman, R. D.; Mrksich, M. Geometric control of vimentin intermediate filaments. *Biomaterials* **2014**, *35*, 1359–1366.

(14) Robison, P.; Caporizzo, M. A.; Ahmadzadeh, H.; Bogush, A. I.; Chen, C. Y.; Margulies, K. B.; Shenoy, V. B.; Prosser, B. L. Detyrosinated microtubules buckle and bear load in contracting cardiomyocytes. *Science* **2016**, *352*, aaf0659.

(15) Liu, C.-Y.; Lin, H.-H.; Tang, M.-J.; Wang, Y.-K. Vimentin contributes to epithelial-mesenchymal transition cancer cell mechanics by mediating cytoskeletal organization and focal adhesion maturation. *Oncotarget* **2015**, *6*, 15966–15983.

(16) Schaedel, L.; Lorenz, C.; Schepers, A. V.; Klumpp, S.; Köster, S. Vimentin intermediate

bioRxiv preprint doi: https://doi.org/10.1101/2023.04.19.537509; this version posted April 21, 2023. The copyright holder for this preprint (which was not certified by peer review) is the author/funder, who has granted bioRxiv a license to display the preprint in perpetuity. It is made available under aCC-BY-NC-ND 4.0 International license.

filaments stabilize dynamic microtubules by direct interactions. *Nat. Commun.* **2021**, *12*, 3799.

(17) Salomon, A. K.; Phyo, S. A.; Okami, N.; Heffler, J.; Robison, P.; Bogush, A. I.; Prosser, B. L. Desmin intermediate filaments and tubulin detyrosination stabilize growing microtubules in the cardiomyocyte. *Basic Res. Cardiol.* **2022**, *117*, 53.

(18) Gurland, G.; Gundersen, G. G. Stable, detyrosinated microtubules function to localize vimentin intermediate filaments in fibroblasts. *J. Cell Biol.* **1995**, *131*, 1275–1290.

(19) Waterman-Storer, C. M.; Salmon, E. Actomyosin-based Retrograde Flow of Microtubules in the Lamella of Migrating Epithelial Cells Influences Microtubule Dynamic Instability and Turnover and Is Associated with Microtubule Breakage and Treadmilling. *J. Cell Biol.* **1997**, *139*, 417–434.

(20) Brangwynne, C. P.; MacKintosh, F. C.; Weitz, D. A. Force fluctuations and polymerization dynamics of intracellular microtubules. *Proc. Natl. Acad. Sci. USA* **2007**, *104*, 16128–16133.

(21) Bicek, A. D.; Tüzel, E.; Demtchouk, A.; Uppalapati, M.; Hancock, W. O.; Kroll, D. M.; Odde, D. J. Anterograde Microtubule Transport Drives Microtubule Bending in LLC-PK1 Epithelial Cells. *Mol. Biol. Cell* **2009**, *20*, 2943–2953.

(22) Brangwynne, C. P.; MacKintosh, F. C.; Kumar, S.; Geisse, N. A.; Talbot, J.; Mahadevan, L.; Parker, K. K.; Ingber, D. E.; Weitz, D. A. Microtubules can bear enhanced compressive loads in living cells because of lateral reinforcement. *J. Cell Biol.* **2006**, *173*, 733–741.

(23) Alisafaei, F.; Mandal, K.; Swoger, M.; Yang, H.; Guo, M.; Janmey, P. A.; Patteson, A. E.; Shenoy, V. B. Vimentin Intermediate Filaments Can Enhance or Abate Active Cellular Forces in a Microenvironmental Stiffness-Dependent Manner. **2022**, preprint posted April 4, 2022.

bioRxiv preprint doi: https://doi.org/10.1101/2023.04.19.537509; this version posted April 21, 2023. The copyright holder for this preprint (which was not certified by peer review) is the author/funder, who has granted bioRxiv a license to display the preprint in perpetuity. It is made available under aCC-BY-NC-ND 4.0 International license.

(24) Colucci-Guyon, E.; Portier, M.-M.; Dunia, I.; Paulin, D.; Pournin, S.; Babinet, C. Mice lacking vimentin develop and reproduce without an obvious phenotype. *Cell* **1994**, *79*, 679–694.

(25) Breuer, D.; Nowak, J.; Ivakov, A.; Somssich, M.; Persson, S.; Nikoloski, Z. System-wide organization of actin cytoskeleton determines organelle transport in hypocotyl plant cells. *Proc. Natl. Acad. Sci. USA* **2017**, *114*, E5741–E5749.

(26) Marcotti, S.; Belo de Freitas, D.; Troughton, L. D.; Kenny, F. N.; Shaw, T. J.; Stramer, B. M.; Oakes, P. W. A Workflow for Rapid Unbiased Quantification of Fibrillar Feature Alignment in Biological Images. *Front. Comput. Sci.* **2021**, *3*, 745831.

(27) Park, S. R.; Kolouri, S.; Kundu, S.; Rohde, G. K. The cumulative distribution transform and linear pattern classification. *Appl. Comput. Harmon. Anal.* **2018**, *45*, 616–641.

(28) Eckes, B.; Dogic, D.; Colucci-Guyon, E.; Wang, N.; Maniotis, A.; Ingber, D.; Merckling, A.; Langa, F.; Aumailley, M.; Delouvée, A.; Koteliansky, V.; Babinet, C.; Krieg, T. Impaired mechanical stability, migration and contractile capacity in vimentin- deficient fibroblasts. *J. Cell Sci.* **1998**, *111*, 1897–1907.

(29) Saldanha, R.; Thanh, M. T. H.; Krishnan, N.; Hehnly, H.; Patteson, A. Vimentin impacts centrosome function and microtubule acetylation. **2023**, preprint posted February 18, 2023.

(30) Pallavicini, C.; Monastra, A.; Bardeci, N. G.; Wetzler, D.; Levi, V.; Bruno, L. Characterization of microtubule buckling in living cells. *Eur. Biophys. J.* **2017**, *46*, 581–594.

(31) Rauch, P.; Heine, P.; Goettgens, B.; Käs, J. A. Forces from the rear: deformed microtubules in neuronal growth cones influence retrograde flow and advancement. *New J. Phys.* **2013**, *15*, 015007.

bioRxiv preprint doi: https://doi.org/10.1101/2023.04.19.537509; this version posted April 21, 2023. The copyright holder for this preprint (which was not certified by peer review) is the author/funder, who has granted bioRxiv a license to display the preprint in perpetuity. It is made available under aCC-BY-NC-ND 4.0 International license.

(32) Chakraborty, S.; Mahamid, J.; Baumeister, W. Cryoelectron Tomography Reveals Nanoscale Organization of the Cytoskeleton and Its Relation to Microtubule Curvature Inside Cells. *Structure* **2020**, *28*, 1–13.

(33) Pallavicini, C.; Levi, V.; Wetzler, D. E.; Angiolini, J. F.; Benseñor, L.; Despósito, M. A.; Bruno, L. Lateral motion and bending of microtubules studied with a new single-filament tracking routine in living cells. *Biophys. J.* **2014**, *106*, 2625–2635.

(34) Guo, M.; Ehrlicher, A. J.; Mahammad, S.; Fabich, H.; Jensen, M. H.; Moore, J. R.; Fredberg, J. J.; Goldman, R. D.; Weitz, D. A. The role of vimentin intermediate filaments in cortical and cytoplasmic mechanics. *Biophys. J.* **2013**, *105*, 1562–1568.

(35) Lee, T.; Kashyap, R.; Chu, C. Building Skeleton Models via 3-D Medial Surface Axis Thinning Algorithms. *CVGIP: Graphical Models and Image Processing* **1994**, *56*, 462–478.

(36) Cameron, A. C.; Gelbach, J. B.; Miller, D. L. Bootstrap-Based Improvements for Inference with Clustered Errors. *Rev. Econ. & Stat.* **2008**, *90*, 414–427.